

Vat 3D Printing of Full-Alginate Hydrogels via Thiol-Ene Reactions towards Tissue Engineering Applications

Michael Zanon^{a,b}, Laura Montalvillo-Jiménez^b, Raquel Cue-López^{b,d}, Enrique Martínez-Campos^{b,d}, Marco Sangermano^c, Annalisa Chiappone^{e*}, Paula Bosch^b

^aCenter for Sustainable Future Technologies (CSFT)@Polito, Istituto Italiano di Tecnologia, Via Livorno 60, Torino, 10144, Italy

^bDepartamento de Química Macromolecular Aplicada, Instituto de Ciencia y Tecnología de Polímeros, Consejo Superior de Investigaciones Científicas (CSIC), C/Juan de la Cierva 3, Madrid, 28006, Spain

^cDipartimento di Scienza Applicata e Tecnologia, Politecnico di Torino, C.so Duca degli Abruzzi 24, 10129 Turin, Italy

^dGrupo de Síntesis Orgánica y Bioevaluación, Instituto Pluridisciplinar (UCM), Unidad Asociada al ICTP, IQM (CSIC), Paseo de Juan XXIII 1, Madrid, 28040, Spain

^eDipartimento di Scienze Chimiche e Geologiche, Università degli studi di Cagliari, Via Università 40, 09124 Cagliari, Italy

Keywords: Alginate, click chemistry, thiol-ene reactions, Hydrogels, 3D printing, DLP, tissue engineering

Abstract

The rise of 3D printing gave an important pulse into the medical field, envisaging the possibility to create artificial engineered tissues/organs perfectly suiting the patients' tissues defects while using their own cells; this approach could in the future respond to the lack of tissues donors and decrease the possible dangerous tissue rejection. Different 3D printing technologies can be considered for the building of scaffolds; despite these promises, very few inks for light-induced 3D printing are nowadays available on the market. Herein for the first time, the alginate backbone is completely functionalized with thiol and alkene groups (separately) to create an innovative full-alginate ink for digital light processing (DLP) printers, using the more biocompatible thiol-ene reactions instead of (meth)acrylic photochemistry and without any addition of small crosslinkers to the printable formulation. Simple synthetic "two-reactions" or "one-pot" strategies are explored to functionalize alginate with thiol/alkene groups able to undergo click reactions. High levels of reproducibility of the modification strategy are obtained. The hydrogels are characterized studying their formulation reactivity, mechanical properties, swelling kinetic and morphological appearance, placing the resulted hydrogel into the stiffer scaffolds category. The selected hydrogel formulation, tested as ink for DLP 3D printing, demonstrates good processability and geometry fidelity with the possibility to form 3D suspended structures. At the end, cells attachment and proliferation are evaluated on the hydrogel, certifying the possible use of the ink for the creation of tissues/organs substitutes (e.g., intestines or tendons) in tissue engineering applications.

Introduction

Photo-polymerization is a well-known crosslinking method that keeps gaining increasing interest in a large number of fields, such as paint and coatings^{1, 2}, sealings^{3, 4}, electronics⁵⁻⁷ or orthodontics⁸⁻¹⁰. Especially in the biomedical field, photo-polymerization emerged as one of the most efficient and versatile processes to produce chemically crosslinked polymers^{11, 12}; rapid times of reaction upon light exposure (UV or visible), good spatio-temporal control of the forming polymer and the possibility to perform the reaction under physiological conditions (e.g., pH or temperature) make the technology highly attractive for the field^{13, 14}.

Indeed, tissue engineering applications are currently trying to exploit the creation of photocurable hydrogels able to replace damaged or failed soft tissues/organs. 3D printing, as the natural evolution of photo-polymerization processes, might assist in accomplishing this challenge by forming tailored scaffolds based exactly on the patient needs¹⁴⁻¹⁶. Starting from their computer-aided design (CAD) customized fabrication, 3D printing techniques are commonly more cost-efficient and faster than traditional manufacturing technologies^{17, 18}. These technologies can be divided in two main categories: extrusion-based and lithography-based 3D printers¹⁹. While extrusion-based technologies are known for their enhanced versatility (e.g., fused direct ink write and fused deposition modelling printers), lithography-based techniques permit the creation of complex and interconnected architectures with the best resolution overall²⁰. In particular, digital light processing (DLP) printers are able to create every entire layer all-at-once thanks to a micro-mirrors system¹⁴, reducing the production time.

Hydrogels are among the most studied materials in tissue engineering²¹ and their shaping by 3D printing is still an open challenge. Aiming to mimic the proteins-glycosaminoglycans blend of the human extracellular matrix (ECM)²², polysaccharides are generally accepted as valid candidates²³. In detail, alginate has been extensively studied and employed for a large number of biomedical applications, due to its biocompatibility, low toxicity and relatively low cost²⁴. It is typically extracted from brown algae, and it is composed of regions of sequential (1-4)-linked β-D-mannuronic acid (M-blocks) monomers, regions of sequential α-L-guluronic acid (G-blocks) monomers, and regions of not tactically organized M and G units. The structure (i.e., repetitive units' composition), abundance and length of the different blocks are extremely important, as they will determine the physical properties of the hydrogel^{21, 25, 26, 27}. In any case, both blocks comprise carboxylic moieties able to deprotonate at physiological conditions, resulting in a perfectly water-soluble natural polymer (the minimum in solubility is around a pH of 3-3,5 due to the protonation of the carboxylic groups and the polar interactions onset)²⁶.

Aiming to gather the appealing properties of alginate with the advantages of photopolymerization and lithography-based 3D printing, photocurable reactive groups must be grafted on the polymer chain. Even if many natural polymers have been modified with acrylic/methacrylic groups to perform fast radical chain growth photopolymerization reactions^{28, 29}, step growth propagation reactions are nowadays experiencing an increasing interest. In fact, the main advantages of these reactions are the lower stress accumulation once the 3D hydrogel is formed, the lower cytotoxicity and enhanced chemoselectivity of the reacting moieties³⁰⁻³². In these circumstances, especially “click chemistry” reactions are exploited because of their rapidity, versatility, regioselectivity, easy usability, as much as their high yields achievable under mild conditions³³⁻³⁵. Despite the fact that thiol-ene are known to be biocompatible photo-induced reactions³⁶⁻³⁸, thiomers gained increased popularity in the last decade in the biomedical field mainly for drug delivery applications (due to their mucoadhesive properties)³⁹⁻⁴¹ but not much for tissue engineering applications⁴²⁻⁴⁴. Within this framework, many synthetic protocols were reported in the last years to functionalize alginate with thiol moieties⁴⁵⁻⁴⁷, but no big attention was given to the maximization of the degree of

functionalization (essential if pursuing a photo-activated crosslinking via thiol-ene reactions). Strictly concerning alginate photo-crosslinking, to the best of our knowledge, just few publications focused on the creation of photocured thiol-ene/yne alginate hydrogels are available and these report the use of ene/yne modified alginate and synthetic dithiol molecules to obtain the crosslinking^{31,35}. Herein due to its easy modification, sodium alginate is selected to create soft hydrogels thanks to its high quantity of carboxylic moieties (compared with chitosan, hyaluronic acid, cellulose, etc.)⁴⁸. Different polysaccharide batches are modified separately with alkene and thiol groups investigating different functionalization procedures and bringing to different degree of functionalization toward the creation of hydrogels. Indeed, this work's intention resides on the exploration of simple synthetic routes to functionalize alginate with thiol/alkene groups able to undergo click reactions (exploiting both "one-pot" and "two reaction" strategies) for the development of alginate photocurable inks presenting the suitable characteristics in terms of viscosity, reactivity and mechanical properties, for the LP printing of 3D structures. In this way, a full alginate network can be created via thiol-ene reaction without the addition of any external crosslinking molecule. It is shown that the straightforward one-pot strategy allows the reaching of suitable degrees of functionalization on the alginate backbone both for thiols and ene functionalities: appropriate crosslinking is achieved to meet the mechanical properties required both for tissue engineering and DLP printing. Furthermore, good values of cells adhesion and proliferation ensure an enhanced biocompatibility of the hydrogels, resulting in appropriate candidates for the production of 3D scaffolds in tissue engineering applications.

Experimental

Materials

Alginic acid sodium alginate from brown algae (SA, low viscosity), Cysteamine hydrochloride (CSA, $\geq 98\%$), L-Cysteine (CYS, 97%), Sodium Periodate (ACS reagent, $\geq 99.8\%$), sodium borohydride (powder, $\geq 98\%$), Sodium nitrate (ACS reagent, $\geq 99.0\%$), N-(3-Dimethylaminopropyl)-N'-ethylcarbodiimide hydrochloride (EDC, $\geq 98\%$), N-Hydroxysuccinimide (NHS), lithium phenyl-2,4,6-trimethylbenzoylphosphinate (LAP, $\geq 95\%$), hydrochloric acid solution (37%), Hydroxylamine hydrochloride (ACS reagent, 98.0%), Methyl orange (for microscopy), phosphate buffer solution tablets (PBS buffer, BioUltra, pH 7.4), 2-Morpholinoethanesulfonic acid monohydrate (MES buffer, Millipore) sodium phosphate monobasic (reagentplus, $\geq 99.0\%$), sodium phosphate dibasic (reagentplus, $\geq 99.0\%$), Ethylenediaminetetraacetic acid (EDTA, BioUltra, anhydrous, $\geq 99\%$) 5,5'-Dithiobis(2-nitrobenzoic acid) (DTNB or Ellman reagent, suitable for determination of sulfhydryl groups, $\geq 98\%$) were all purchased from Sigma-Aldrich and used as received without further purification. Sodium hydroxide pellets were purchased from Panreac, pre-wetted dialysis membranes (MWCO 3500 Da Spectra/Por6) from Spectrum Laboratories and 5-Norbornene-2-methylamine (NOR, mixture of isomers) from TCI Europe N.V.

Two-reactions thiolation strategy

1. Synthesis of Oxidized Sodium Alginate (OSA)

Alginate was oxidized using different molar ratios between the alginate polysaccharide unit and sodium periodate (i.e., 5:1, 10:1, 20:1) for 3 h, following the procedure described by Huamani-Palomino et al,⁴⁵. Briefly, in a round bottom flask 0.5 g of Sodium Alginate were solubilized in 25 ml of distilled water (DI water) by stirring overnight at RT (2 % w/v). Then, 25mL of a sodium periodate solution were added to the alginate solution while stirring at room temperature into darkness. Concentration of this solution was fixed in each case to obtain the desired molar ratio between SA and NaIO₄. The reaction was quenched after 30 min with a

10% v/v solution of ethylene glycol in DI water, while stirring⁴⁸. The product was isolated by dialysis against water during 6 days with a 3.5 KDa membrane and dried by rotary evaporation at 37°C.

2. *Synthesis of Thiolated Oxidized Sodium Alginate (TOSA)*

The thiolation procedure was performed as reported in literature⁴⁵. Firstly, in a round bottom flask 0.5 g of freeze-dried OSA was dissolved in 40 mL of 0.1 M phosphate buffer solution (PBS, 1.25 % w/v at pH 7.4). At the same time, 1.2 g of cysteine (molar ratio of 1:4 between the alginate units and cysteine) were solubilized in 10 mL of water and added to OSA solution. Finally, the mixture was stirred at room temperature for 24 h in the darkness, under nitrogen atmosphere⁴⁹. Then, 0.4 g of sodium borohydride NaBH₄ were added to the solution and the reaction was stirred in the darkness for another 15 h at room temperature under nitrogen atmosphere. The product (TOSA, Thiolated Oxidized Sodium Alginate) was isolated by dialysis against water (6 days) in the darkness at 10° C with a 3.5 KDa membrane against saline acidic DI water (pH 4 and 0,1 M of NaCl).

One-Pot synthesis of sodium alginate-cysteine and sodium alginate-cysteamine conjugates (SA-CYS and SA-CSA)

0.5 g of SA were solubilized previously in 33 ml of DI water into a round bottom flask (1.5 % w/v). Few drops of HCl solution were added until pH=4. Then, a solution of EDC/NHS (1.568 g/1.163 g, 4 equivalents to SA carboxylic groups) in DI water was added dropwise. Then the pH was adjusted to a value of 4. The solution was allowed to stir 2 h at RT and under N₂ atmosphere to activate the carboxylic groups of alginates. The pH was then adjusted to 4 if needed. 1.223 g of CYS or 1.148 g of CSA (4 equivalents to SA carboxylic groups) were solubilized in DI water and added to the solution with a syringe. The reaction was maintained in the darkness under stirring and N₂ atmosphere at RT for 24 h. The products were then dialyzed 6 days in the darkness at 10°C with a 3,5 KDa membrane against saline acidic DI water (pH 4 and 0,1 M of NaCl) to avoid thiol oxidation and disulfide bond creation^{50, 51}.

One-Pot functionalization of Alginate with alkene groups (SA-NOR)

First, 0.5 g of SA were solubilized in MES buffer (0.1 M) into a round bottom flask (2 % w/v). The pH was then lowered with the HCl solution at a value of 4. In a vial, EDC and NHS were solubilized together in MES buffer³¹ (0.940 g/0.232 g, 2.4/0.8 equivalents to SA carboxylic groups, respectively) and slowly added dropwise onto alginate solution. Then the pH was adjusted with the HCl solution until a value of 4. The reaction was stirred 2 h at RT to activate the carboxylic groups of alginates. The pH was then raised to 8.5 with a 0.1 M solution of NaOH. NOR was added directly into the flask under Argon atmosphere (0.311 g, 1 equivalent to SA carboxylic groups). The reaction was performed in the darkness under stirring and under Argon atmosphere at RT for 24. At the end of the reaction the color of the solution was yellowish. The product was then dialyzed 6 days against DI water at RT in the darkness with a 3,5 KDa membrane.

Preparation of the photocurable hydrogel

A 10 wt% solution containing the two functionalized products was prepared by dissolving SA-CSA and SA-NOR 2 separately and then mixing them together until reaching a homogeneous formulation. Then, 1 phr of LAP was added to the solution and let stir until complete dissolution in the darkness. The formulation was then casted in molds of PDMS ($\approx H = 3$ mm, $D = 5$ mm), irradiated 5 min at 50 mW/cm² with a visible light lamp (Hamamatsu LC8) furnished with a cut-off filter for $\lambda < 400$ nm.

Vat 3D-Printing

3D printing was performed with an Asiga PICO 2 DLP-3D printer (Asiga, Australia) equipped with a LED light source emitting at 405 nm (nominal XY pixel resolution is 39 μm , achievable Z-axis control is 1 μm). After printing, the 3D geometries were immersed in distilled water for 1 min and post-cured with a mercury lamp provided by Robotfactory (10 min, light intensity 10 mW/cm^2).

Characterization

Potentiometric evaluation of Aldehyde content

The titration procedure was performed following a previous reported method⁵². A 0.25 M solution of hydroxylamine hydrochloride was prepared firstly adding 0.96 g to 10 ml of DI water while stirring for 30 min. Once reached complete dissolution, 300 μL of a methyl orange solution (1.5 mM) were added. Lastly the solution was topped with DI water to reach 50 ml and adjusted at pH 4. Then, 20 mg of the OSA samples were dissolved in 5 ml of the titration solution where different amount of a NaOH solution (0,1 M) were added while measuring the pH (SI for the detailed description).

Thiol content evaluation (Ellman reagent titration)

The content of free thiol groups was evaluated by the Ellman's reagent method^{53, 54}. A pH 8 phosphate buffer (0,1 M) solution was prepared while EDTA (0,001 M) was added to impede metal chelation of the thiol groups. Separately, 4 mg of DTNB (i.e., Ellman reagent) were solubilized manually in 1 ml of phosphate buffer. In the meantime, various quantities of TOSA/SA-CSA/SA-CYS (around 10 mg) were added into a 5 ml vial of buffer. Then, two UV-VIS cuvettes (blank and sample) were prepared with the indicated proportion:

- 1) Blank: 2,5 ml of buffer + 50 μL of Ellman reagent solution + 250 μL of buffer
- 2) Sample: 2,5 ml of buffer + 50 μL of Ellman solution + 250 μL of TOSA/SA-CSA/SA-CYS solution

This procedure was performed in triplicate measuring the light absorption at 412 nm (SI for details).

Nuclear magnetic resonance spectroscopy analysis (¹H-NMR and solid-state ¹³C-NMR)

¹H-NMR spectra was recorded on a Bruker Avance 400 MHz and on a Varian Mercury 400 MHz spectrometers with samples dissolved in D₂O at room temperature. The reference for the integration has always been the whole signal of Sodium Alginate skeleton, considering that it corresponds to 4 protons of the pyranose ring. The solid state NMR were registered in a Bruker Avance 400 spectrometer equipped with a 89 mm wide bore, 9.4 T super-conducting magnet (proton Larmor frequency at 400.14 MHz). The reported data were recorded at room temperature using cross polarization (CP), magic-angle spinning (MAS), high-power ¹H decoupling and a rotor spinning rate of 5KHz. The contact time was set to 3 ms, and recycle time between subsequent acquisitions was set to 3 s. The spectral width was 35 KHz and adamantane was used as the external chemical shift reference. The obtained spectra were in both cases evaluated by MestReNova software.

Gel Permeation Chromatography (GPC)

The molecular weight of commercial SA and its derivatives (oxidized sodium alginate, OSA) was determined by size exclusion chromatography (GPC) using a Shimadzu modular system comprising: DGU-20A3 solvent degasser, LC-20AD pump, column oven, HT- autosampler 20A HT, and RID-10A refractive index detector. The samples were dissolved (2 mg/mL) in the mobile phase based on Milli-Q water with NaNO₃ (0.2 M).

ThermoGravimetric Analysis (TGA)

[...]

Hydrogel characterization

Real-time photorheological measurements were performed using an Anton PAAR Modular Compact Rheometer (Physica MCR 302, Graz, Austria) in parallel-plate mode (25 mm diameter) and the visible-light source was provided by positioning the light guide of the visible Hamamatsu LC8 lamp under the bottom plate. During the measurements, the gap between the two glass plates was set to 0.2 mm, and the sample was kept under a constant shear frequency of 1 Hz. The irradiating light was switched on after 60 s to allow the system to stabilize before the onset of polymerization. According to preliminary amplitude sweep measurements, all the tests were carried out in the linear viscoelastic region at a strain amplitude of 5%. The photorheology was studied as a function of the changes in the shear modulus (G') and in the loss modulus (G'') of the sample versus the exposure time. Amplitude sweep tests were performed on the cured hydrogels in the range between 1 and 1000% of strain, frequency of 1 Hz. The mechanical properties were measured by a dynamic compression test. Measurements were performed on swelled 3D printed cylindrical scaffolds ($\approx h = 3$ mm, $d = 5$ mm) at 25 °C and using a universal test system, MTS QTest1/L Elite, a uniaxial testing machine equipped with a 100 N load cell in compression mode. Samples were placed between compression platens. Each sample was subsequently deformed at 1 mm/min. **The storage modulus E' was calculated on the first 10% of deformation.** All measurements were performed by triplicate. The different photocured samples ($\approx h = 3$ mm, $d = 5$ mm) were washed and let dry overnight. Once dry, the samples were weighted and soaked in DI water to evaluate the swelling capability and kinetics. The samples were taken out at different time intervals and weighted once the surface droplets were wiped off with wet paper until constant weight. The swelling ratio ($Sw\%$) was calculated as:

$$Sw (\%) = \frac{W_t - W_0}{W_0} * 100 \quad (1)$$

W_t is the weight of the hydrogel sample at a specific time, and W_0 is the weight of the dried sample recorded as the initial weight. All tests were performed in triplicate. To determine the gel content (GC), previously dried samples were held in a metal net, weighed, and then immersed in DI water (25°C) for 24 h to dissolve the uncrosslinked polymer. The samples were then dried for 24 hours (40° C) in a vacuum oven and weighed again. The gel content was determined as:

$$GC (\%) = \frac{W_i}{W_f} * 100 \quad (2)$$

Where W_i is the initial weight and W_f the weight after extraction.

The morphological characterization of the samples was carried out by field emission scanning electron microscopy (FESEM, Zeiss Supra 40, Oberkochen, Germany). The hydrogel samples were first frozen, sectioned in half, and lyophilized before coating with a 5 nm thick, thin film of Pt/Pd.

Cell viability and proliferation

Before the cell viability and proliferation assays, all the hydrogels were sterilized in 48-well plate (Corning). The hydrogels were stored in 70% ethanol for a week, and then carefully rinsed with PBS (phosphate buffer solution, Thermo Fisher) and sterilized with ultraviolet germicidal irradiation (UVGI) for 40 min. After a final rinse with PBS, the hydrogels were cover with DMEM 1X (Gibco) supplemented with 10% FBS (fetal bovine serum, Thermo Scientific) plus

antibiotics 100 U mL⁻¹ penicillin and 100 µg/mL streptomycin sulfate (Sigma-Aldrich). After 24h of contact between the culture medium and the hydrogels at 37°C, the media containing soluble extracts was collected and kept in the freezer until further use. Cell assays were performed using C166-GFP mouse endothelial cell line (ATCC CRL-2583™, USA): 20,000 cells/ml were seeded in a 12-well culture plate and allowed to adhere and grow for 24h. Then, the media was changed for a mixture (1:1 and 1:5) of complete DMEM and the medium that had been in contact with the hydrogels. Inverted fluorescence microscopy (Olympus IX51, FITC filter $\lambda_{ex}/\lambda_{em} = 490/525$ nm) was used daily to evaluate any changes in the cell culture morphology and proliferation, that could indicate the leaching of toxics from the hydrogels. After 48h, when the cell cultures reached confluency, metabolic activity of the cells was measured using Alamar Blue assay, following the instructions of the manufacturer (Biosource). This method is non-toxic and uses the natural reducing power of living cells, generating a quantitative measure of cell viability and cytotoxicity. Briefly, Alamar Blue dye (10 % of the culture volume) was added to each well containing living cells and incubated for 90 minutes. Then, the fluorescence of each well was measured using a Synergy HT plate reader (BioTek) at 535/590 nm. Finally, DNA quantitation of cells was determined by FluoReporter® Blue Fluorometric dsDNA Quantitation Kit fluorescent staining. This method is based on the ability of the bisbenzimidazole derivative Hoechst 33258 to bind to A-T-rich regions of double-stranded DNA. After binding to DNA, Hoechst 33258 exhibits an increase in fluorescence, which is measured at 360 nm excitation wavelength and 460 nm emission using a microplate reader (BioTek, Synergy HT).

Results and discussions

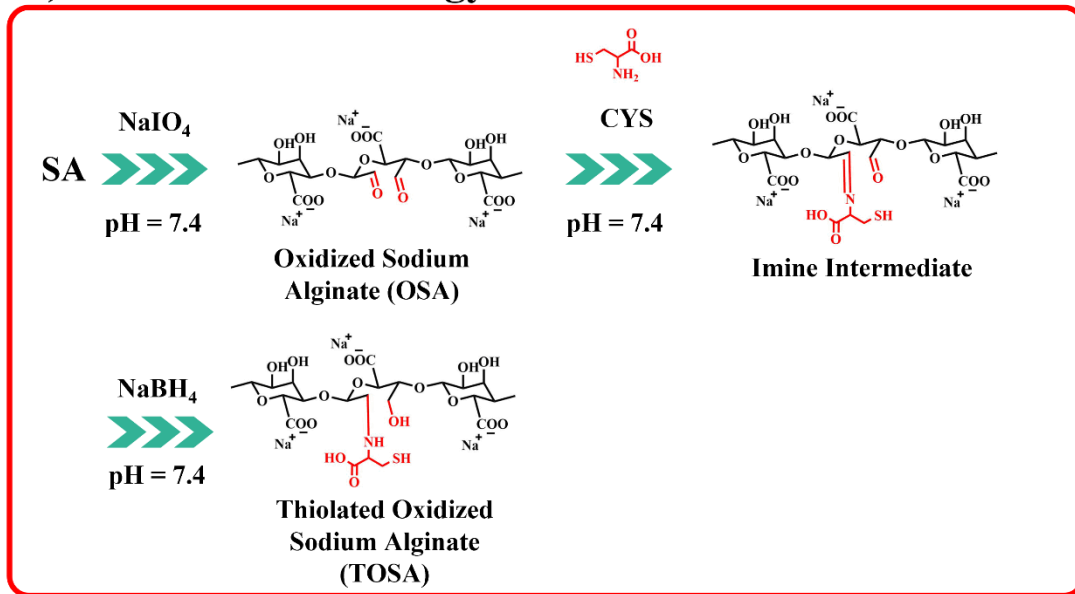
Alginate functionalization reactions

Several routes of functionalization have been proposed to modify alginate (including thiolation reactions): among them, we selected two general strategies which target different chemical species of the alginate backbone: carboxylic groups (based on carbodiimide chemistry^{31, 39}) or oxidation of the ring^{45, 47}. So, different thiolation protocols were firstly explored as summarized in Figure 1; instead, the thiol-ene chemical crosslink reaction is reported in Figure S1.

The first proposed way to functionalize alginate with thiol groups exploits a “two-reactions” strategy which include an initial step of oxidation. Following, alginate is functionalized with cysteine by a spontaneous reaction between the aldehydes and the cysteine secondary amine imine, forming an imine intermediate subsequently reduced by addition of sodium borohydride (scheme on Figure 1 A). The oxidative modification with sodium periodate of alginate is expected to take place on the adjacent C-2 and C-3 hydroxyl groups on the glucose ring, creating a couple of aldehyde moieties on the alginate backbone^{46, 48}. For this step, three different molar ratios between the total carbohydrate rings and the oxidizer (Sodium Periodate) were investigated, resulting in different aldehydes content evaluated by potentiometric titration (See SI). Table 1 reports the molar ratio investigated and the degree of functionalization obtained for this synthesis step. Degrees of functionalization of 33, 10 and 4% for OSA 1, OSA 2 and OSA 3 were obtained respect the total alginate rings (respectively). However, considering that each cleavage on the alginate backbone forms two aldehydes’ moieties, the theoretical degree of functionalization for the three reaction conditions would have been 40, 20 and 10% (respectively on OSA 1, OSA 2 and OSA 3). This lower value found can be explained considering that aldehydes, once formed, are highly reactive and can react with surrounding water molecules giving the more stable hemiacetal form. Especially this reaction can decrease the total number of available aldehyde moieties⁵⁵. In addition, oxidation reactions could also lead to cleavages onto alginate skeleton, lowering the molecular weight of the

polymer (while affecting the final hydrogel stiffness)^{45, 56}. Thus, the three oxidized alginates and the commercial sodium alginate were subjected to gel permeation chromatography to track the molecular weight after reaction.

A) Two reaction strategy



B) "One-Pot" reaction strategy

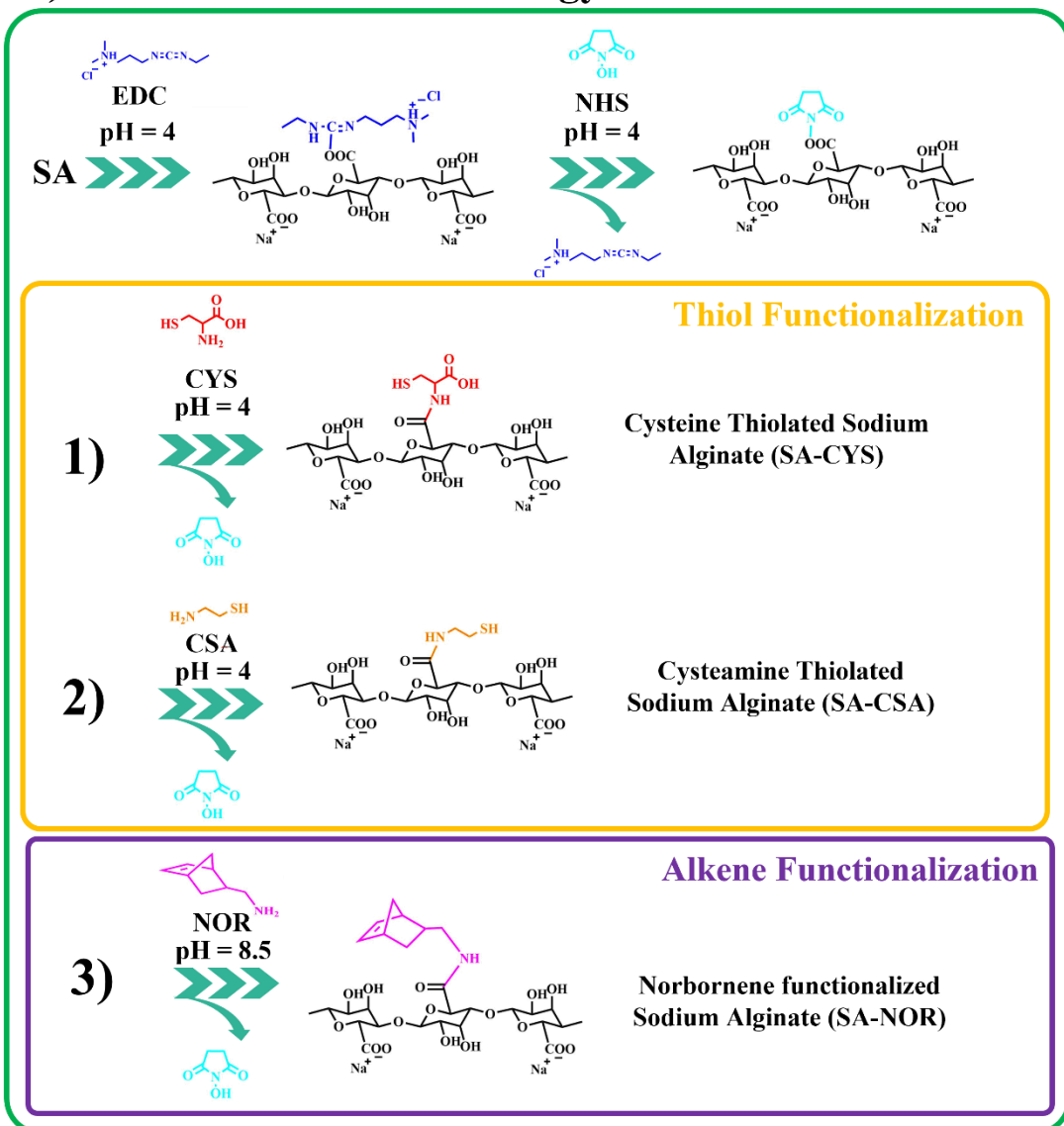


Figure 1: Schemes of the alginate functionalization reactions studied in this work. (A) two- reaction strategy to obtain the thiolated oxidized sodium alginate (TOSA). (B) Carbodiimide chemistry-based “one-pot” strategy to obtain thiolated alginate SA-CYS (1), SA-CSA (2) or alkene-alginate SA-NOR (3).

Table 1 reports the number average molecular weight (M_n), and polydispersity index (M_w/M_n) of SA and the obtained oxidized product. As expected, lower molecular weights are found once higher quantity of oxidizer are used, confirming reactions of chain breaking. Even though the M_w decrease, OSA 1 was chosen for further step of functionalization due to the acceptable final molecular weight, lower polydispersity and its higher level of modification, needed for the next step of thiolation and in line with previous reported works^{45,56}.

Table 1: Molar ratio between the alginic ring and sodium periodate investigated; Degree of functionalization obtained after the oxidative step; Gel permeation chromatography data of sodium alginate (SA) and the three oxidized sodium alginate synthesis batches (OSA).

Sample	Molar ratio (SA:NaIO ₄)	Degree of functionalization (DF%)	M_n	M_w/M_n
OSA 1	5:1	33 ± 1	16228	2.23
OSA 2	10:1	10 ± 1	38686	2.52
OSA 3	20:1	4 ± 1	46131	2.83
SA	--	--	58537	3.33

The presence of aldehyde functional groups on OSA 1 was further confirmed by ATR FT-IR, ¹H-NMR and solid-state ¹³C-NMR (Figure 2). The FT-IR spectra showed the appearance of a new peak around 1720 cm⁻¹, related to the C=O carbonyl stretch of saturated aliphatic aldehydes (Figure 2 A)⁴⁸, while ¹H-NMR (Figure 4 B) and solid-state ¹³C-NMR (Figure 4 C) confirmed the characteristics aldehydes bands at 5.31-5.61 ppm and 92 ppm, respectively^{45,57}.

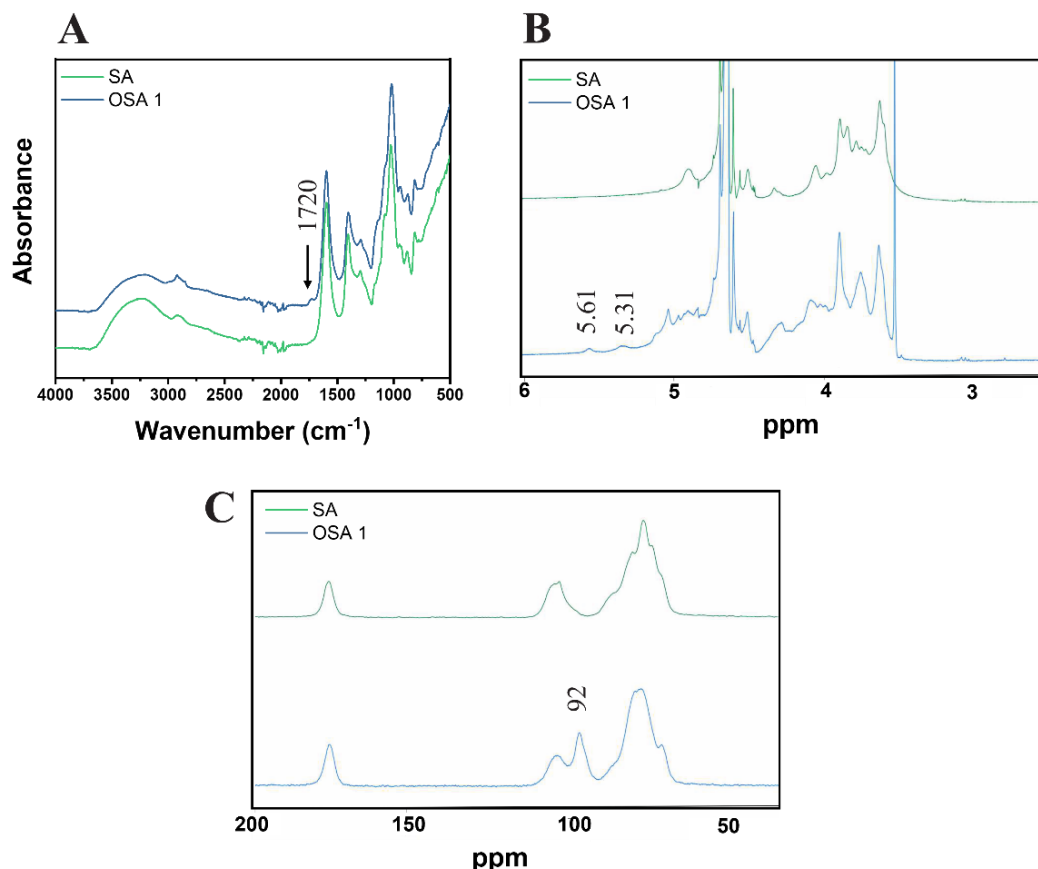


Figure 2: ATR FT-IR (A), $^1\text{H-NMR}$ (B) and solid-state $^{13}\text{C-NMR}$ (C) of OSA 1.

In the second step the thiolation reaction was performed using cysteine (CYS) as reactant^{45,47}, with a molar ratio of 1:4 between the alginate rings and cysteine. The synthesis conditions are also reported in Table S1 (See SI). Briefly, the Schiff base reaction leads to a nucleophilic addition of the cysteine primary amines on the OSA aldehydes⁵⁸. After, the carbinolamine intermediate evolves by dehydration to an imine functionality^{46,59}. The pH was maintained at 7.4 to ensure an effective Schiff base reaction⁶⁰. The reduction of the imine groups by sodium borohydride at a molar 1:1 ratio (compared with the carbonyl groups of OSA) produces thiolated oxidized sodium alginate (TOSA). The degree of substitution was evaluated by the Ellman reagent protocol (see SI). Unfortunately, the degree of functionalization measured by absorption on the UV-VIS spectra resulted into a $0.5 \pm 0.1\%$, evaluated as too low for any further reaction of crosslinking. The lower degree of functionalization of TOSA may be related to a not effective reduction amination reaction and to a subsequent hydrolysis of the imine group during dialysis^{45,61}.

The second synthetic route to functionalize sodium alginate with thiol groups involves the activation of the carboxylic moieties *via* carbodiimide chemistry^{39,62,63} in a “one-pot” strategy (just by adding subsequently the reactants into the same container). The two-step amination reaction employs EDC and NHS as activating agents. In order to compare this reaction with the previously reported one, cysteine (CYS) was selected as functional agent. In addition, to eventually boost further the degree of functionalization, cysteamine (CSA) was also used to modify alginate with thiol moieties. To compare the efficiency of the reactions, the previously used molar ratio between reactants was selected (1:4=SA:CYS or SA:CSA). The reaction schemes are reported in Figure 1 B (1) and (2). Avoiding the oxidation step, the only requirement relates into the control of reaction pH during the different steps. In the first step

(activation of carboxylic groups) an acidic pH is needed (generally around 4), in order to protonate the carboxylic moieties and to make possible the first conjugation with EDC (unstable intermediate) followed by the reaction of NHS to form a stable ester^{64,65}. It is crucial during thiolation the maintenance of a N₂ controlled atmosphere, darkness and acidic pH (i.e., 4), to prevent the easy oxidation of thiols in the presence of oxygen, especially in water environments. Moreover, in water solution, oxygen can also catalyze the formation of disulfide bonds, decreasing the total number of thiol groups^{39,49,50}. The degree of functionalization was measured by the Ellman protocol using the previously reported ϵ (See SI); the used synthesis conditions are summarized in Table S2. SA-CYS showed a degree of functionalization of 4.5 ± 0.3 %, considerably higher than the previous reaction (0.5% = TOSA). Considering the higher degrees of functionalization and the reduction of one purification step, the carbodiimide reaction was selected to functionalize alginate. When used cysteamine (SA-CSA), the degree of functionalization obtained was even higher (14 ± 2 %). In this case, we attribute the increase in modification to the lower steric hindrance of CSA molecule respect to CYS, because of the absence of the second carboxylic group⁴⁵. Considering the results, SA-CSA was chosen as the most promising candidate for the creation of hydrogels.

Given these findings, carbodiimide chemistry was also selected as the strategy to introduce a double bond in alginate skeleton, and norbornene methylamine (NOR) was selected as reactant. The reaction scheme is reported on Figure 1 B (3). In this case, after the similar activation step using EDC and NHS at pH 4 (as described before), the pH was increased until 8.5 to increase the amine nucleophilicity of Norbornene methylamine while making possible its reaction with the intermediate NHS-ester^{61,66,67}; the reaction was maintained under argon atmosphere to prevent self-reaction of the NOR molecules. The synthesis conditions are reported in Table S3 (See SI). Once successfully dialyzed, the product (SA-NOR) was analyzed by ¹H-NMR. The successful functionalization was evidenced by the characteristic peaks at 6.02 and 6.27 ppm in the ¹H-NMR spectrum (Figure 3 A), corresponding at the two methylene of the norbornene double bond³¹. A degree of functionalization of 15% was calculated by integration, value similar to its correlative SA-CSA counterpart. Lastly, the reproducibility of the reactions was evaluated repeating the procedure in triplicate, experiencing similar values of modification for all the products obtained with the “one-pot” strategy (SA-CYS, SA-CSA and SA-NOR) and independently of the functionalization reaction. The degree of functionalization of all the modified alginate are summarized on Figure 3 B. **More information's about the functionalized alginates are reported on SI (ATR-FTIR, ¹H-NMR and ThermoGravimetric Analysis).**

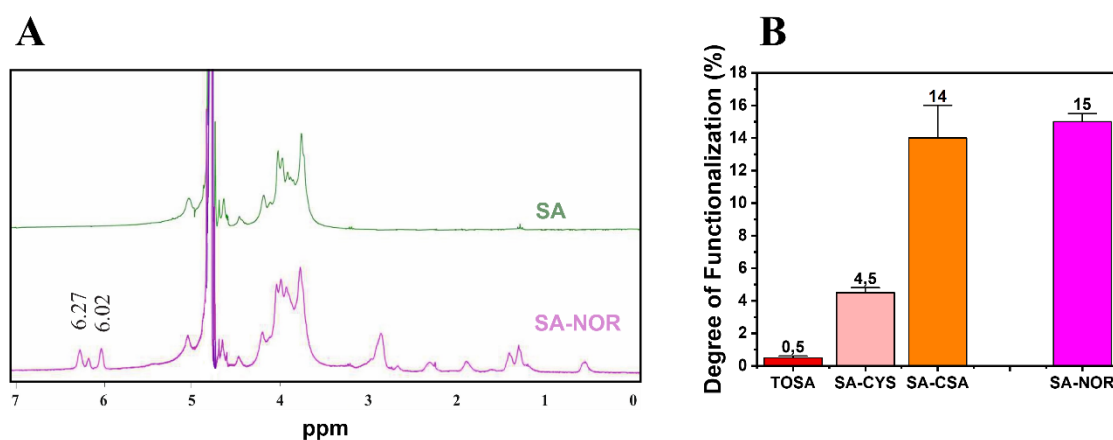


Figure 3: ¹H-NMR spectra of SA-NOR and Sodium Alginate SA (A). Calculated degree of functionalization, obtained by the Ellman's reagent method for the thiolated monomers and by integration of the NMR peaks for SA-NOR (B).

Hydrogel production and characterization

Thiol-ene reactions are known to be highly regiospecific, reactive, and insensitive to oxygen and aqueous environments³⁴. Thus, the two selected products (SA-CSA and SA-NOR) were solubilized separately in DI water at a concentration of 10 wt% and then mixed, expecting a 1:1 regioselective conversion between the thiol and alkene moieties. The total concentration of 10 wt% was chosen according to a preliminary investigation on the viscosity of solutions prepared at different concentration (Figure S4 on SI). Envisaging DLP printing 10wt% resulted a good compromise between viscosity and final mechanical properties⁴⁷ in order to create stiff and self-standing hydrogels. Once having a homogeneous solution, 1 phr (per hundred resin) of LAP photoinitiator was added to the solution and solubilized. The photoinitiator choice resides mainly on the low cytotoxic effects on living cells and its visible light absorption⁶⁸.

The formation of the network, as much as the system reactivity and the irradiation time were investigated by photo-rheology (Figure 4 A). As can be seen, the variation of the storage modulus G' and the loss modulus G'' measured during the photo-crosslinking reaction indicated a high reactive system: absence of reaction delay after light exposure and high slope of storage modulus G' . Also, thiol-ene hydrogel (TE Hydrogel) doesn't show any clear upper plateau even though the reached G' values ($\approx 3 \cdot 10^3$ Pa) are comparable with other reported hydrogel used in tissue engineering⁶⁹⁻⁷¹. This behavior suggests still a slow ongoing progression of the reaction even after 500 s of irradiation. The hydrogel mechanical properties were tested both by amplitude sweep measurements and compression test. The hydrogel stability over an incremental strain is measured by amplitude sweep (Figure 4 B). Herein, an important parameter used to understand the hydrogel properties is the yield point (or the maximum strain point applicable before the hydrogel collapse). This system possesses a yield point at 138% of strain, which is in line or higher with respect to other polysaccharides-based crosslinked hydrogels^{35,69,71,72}. Furthermore, the compressive elastic modulus of 44 ± 3 KPa places the resulted hydrogel among the stiff soft tissue scaffolds, with properties comparable with human intestine or tendons (Figure 4 C)⁷³. Moreover, the low elongation at rupture (27%) and high ultimate strength (≈ 19 KPa) support the brittleness hydrogel observations during amplitude sweep and the theorized high crosslinking density.

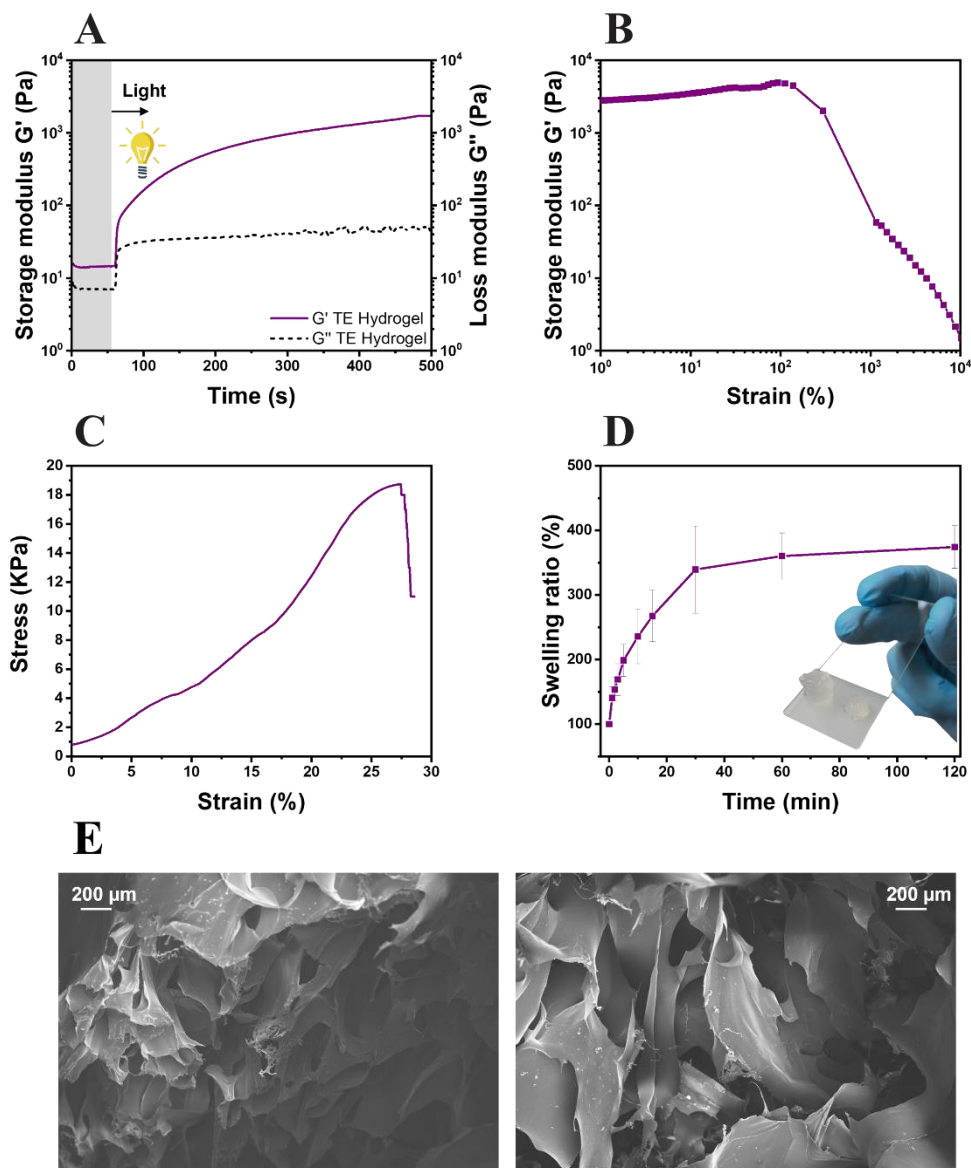


Figure 4: Photo-rheology (A), amplitude sweep (B), compression test (C) and swelling kinetics (D) of the thiol-ene hydrogel (TE hydrogel). Field Emission Scanning Electron Microscopy (FESEM) of the TE hydrogels; scale bar 200 μm (E).

The swelling ability of the hydrogel was also evaluated (Figure 4 D); a swelling equilibrium of $376 \pm 21\%$ was reached after 30 min of immersion in DI water. The results are comparable with data reported on similar studies, both in terms of values and trends of swelling kinetics³¹. The gel content of the hydrogels, assessed in triplicate, showed a value of $78 \pm 3\%$. Both results again suggest the high crosslinking density of the gels. However, known that the scaffolds need to possess a certain degree of porosity to allow cells to attach and migrate inside of the hydrogel, the morphology of the lyophilized hydrogels was investigated by FESEM. As visible on Figure 4 E, the hydrogels possess highly porous structures with diameters in the range of 200 μm , totally compatible with cell dimensions^{74, 75}. Confirmed the high reactivity of the formulation, the hydrogel high yield point and storage modulus at compression, optimal swelling degree and acceptable porosity, the hydrogel was further studied for 3D printing and biological characterization.

Vat 3D-Printing

Considering its high reactivity, the full-alginate formulation was tested for 3D-printing with DLP technology. Beside reactivity the mechanical properties of the cured material are also important during the printing process; indeed, since in DLP printers the final object is built upside-down (scheme on Figure 5), the hydrogel requires sufficient properties of mechanical resistance under low solicitations or strain. The previously measured properties resulted totally comparable with values reported in literature⁶⁹. The printing parameters were empirically optimized and are reported on Table S4 (see SI). As a first attempt, a honeycomb-like structure was printed (Figure 5). This geometry was tested to create shaped bulk structures with thin self-standing walls. As visible, small architectures (around 9.5 mm) were printed with defined angles, forming clear hexagonal cavities (with dimensions of around 3 mm). The ability to create defined structures, both in terms of fidelity and resolution, was then exploited to form suspended architectures. In fact, a stable cubic geometry (named “Hollow cube”) was printed with an internal cavity on the range of 6 mm. Lastly, especially in the upper part of the hydrogel, the angles shape fidelity was extremely high.

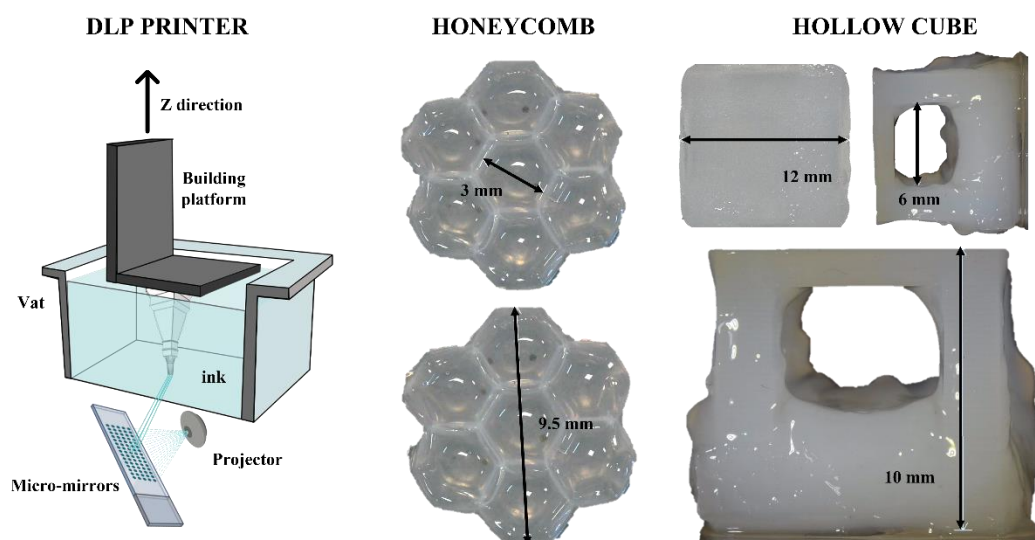


Figure 5: Digital light projection (DLP) printer scheme and the TE hydrogel processed geometries.

Cell viability and proliferation

As described in the characterization methods paragraph, a triplicate of the hydrogel was sterilized and immersed in biological medium at 37° C for 24 h, priorly to the biological evaluation. At the same time, autofluorescent C166-GFP endothelial cells were seeded on a 12-well plate and let adhere for 24 h. The biological medium extracted from the TE hydrogels was brought into contact (1:1 and 1:5 dilutions) with the endothelial cells in the 12-well plate to ensure no toxic substances are released from the hydrogels (according to ISO 10993-5 recommendations). Firstly, cells proliferation was certified over 48 h by inverted field microscopy (Figure 6 A), and then metabolic activity and DNA quantification were assessed to ensure the hydrogels cytocompatibility (Figure 6 B and C, respectively). No evidence of cells detachment, necrotic or apoptotic cells bodies were reported after the culture media replacement but rather the cultures presented healthy and confluent cells monolayers. Compared with the control without extracts, proper levels of mitochondrial metabolic activity were evidenced (Alamar blue assay, Figure 6 B) as much as optimal levels of DNA content, verifying that no cytotoxic substances that could disrupt cell viability were released from the hydrogels (Figure 6 C). Summarizing, the fully modified alginate hydrogel obtained by thiol-

ene reaction did not present any signs of indirect in vitro cytotoxicity and may be used as stiff scaffolds for tissue engineering applications.

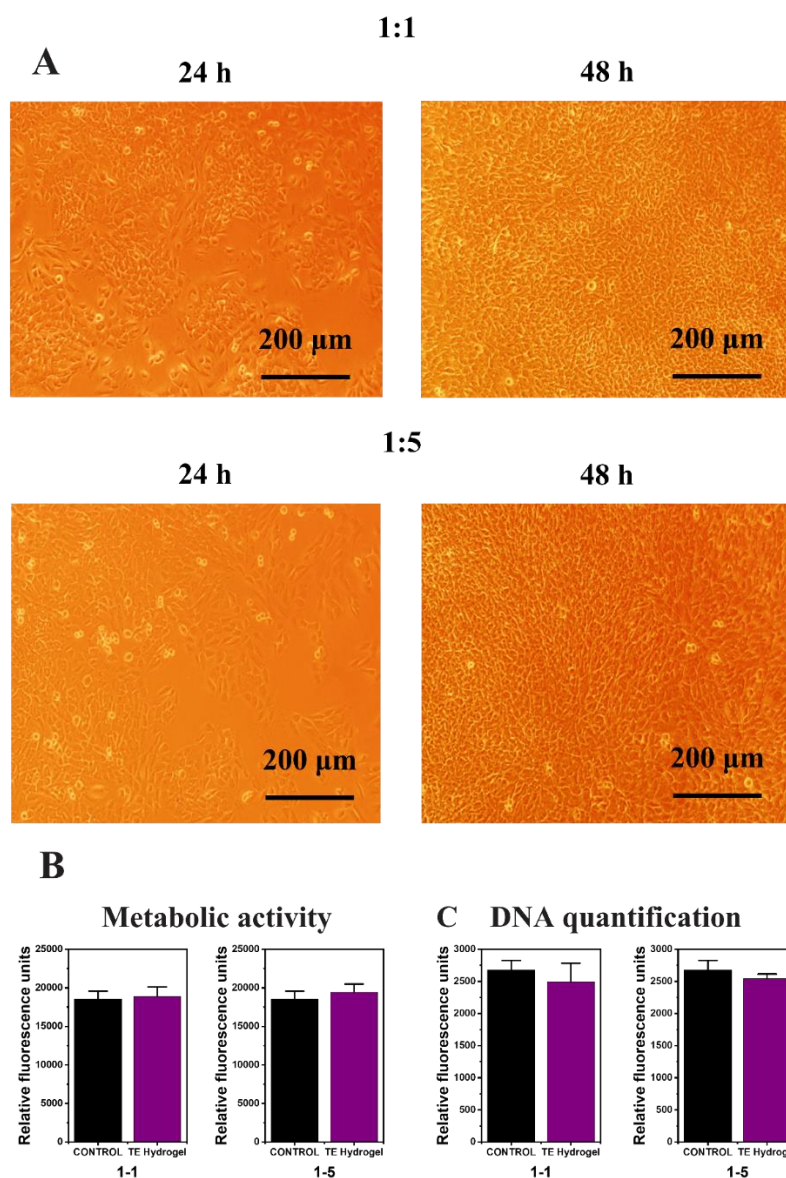


Figure 6: Bright field microscopy (A), metabolic activity (B) and DNA quantification (C) of the TE Hydrogel.

Conclusions

Herein, a simple synthetic route was described to functionalize alginate with both thiol and alkene groups, with the aim to undergo thiol-ene click reactions without the addition of any external crosslinker molecule. Concerning the thiol functionalization, a “two reaction strategy” including the oxidation of the alginate chain and a “one-pot strategy” based on carbodiimide chemistry were evaluated. The best degree of functionalization was achieved using the “one-pot” strategy in presence of cysteamine as functionalizing agent (~ 14%). Then, the same chemical route was selected to incorporate norbornene methylamine, obtaining products with functionalization ranges of the same degree (~ 15%). More importantly, high levels of reactions reproducibility were evidenced, independently of the employed functional molecule. The formulation reactivity was studied by photo-rheology which confirmed the adequacy of the ink properties for DLP 3D printers. The resulted 3D printed structures presented defined and self-

standing hydrogel architectures, with well-shaped angles/surfaces and the possibility to create suspended geometries. The mechanical, swelling and morphological properties of the hydrogels were also evaluated, placing the material among the stiff soft tissue scaffolds, with properties comparable with human intestine or tendons. Furthermore, the modified alginate hydrogel obtained by thiol-ene reaction did not present any signs of indirect in vitro cytotoxicity, suggesting its feasible employment as stiff scaffolds for tissue engineering applications.

References

1. K. D. Weiss, *Progress in Polymer Science (Oxford)*, 1997, **22**, 203-245.
2. F. Peltier and D. Thierry, *Coatings*, 2022, **12**.
3. M. S. Malik, S. Schlögl, M. Wolfahrt and M. Sangermano, *Polymers*, 2020, **12**.
4. B. A. Suslick, J. Hemmer, B. R. Groce, K. J. Stawiasz, P. H. Geubelle, G. Malucelli, A. Mariani, J. S. Moore, J. A. Pojman and N. R. Sottos, *Chemical Reviews*, 2023, **123**, 3237-3298.
5. U. Zschieschang, H. Klauk and J. W. Borchert, *Advanced Materials Technologies*, 2023, **8**.
6. A. G. MacDiarmid, *Angewandte Chemie - International Edition*, 2001, **40**, 2581-2590.
7. Y. K. Yang, *Microelectronics International*, 2006, **23**, 26-32.
8. I. Kunio and E. Takeshi, *Dental Materials Journal*, 2010, **29**, 481-501.
9. F. Petko, A. Świeży and J. Ortyl, *Polymer Chemistry*, 2021, **12**, 4593-4612.
10. A. Santini, I. T. Gallegos and C. M. Felix, *Primary dental journal*, 2013, **2**, 30-33.
11. I. Chiulan, E. B. Heggset, Ş. I. Voicu and G. Chinga-Carrasco, *Biomacromolecules*, 2021, **22**, 1795-1814.
12. C. Felipe-Mendes, L. Ruiz-Rubio and J. L. Vilas-Vilela, *Emergent Materials*, 2020, **3**, 453-468.
13. M. Zanon, D. Baruffaldi, M. Sangermano, C. F. Pirri, F. Frascella and A. Chiappone, *European Polymer Journal*, 2021, **160**.
14. V. S. D. Voet, J. Guit and K. Loos, *Macromolecular Rapid Communications*, 2021, **42**, 2000475.
15. M. Pagac, J. Hajnys, Q.-P. Ma, L. Jancar, J. Jansa, P. Stefek and J. Mesicek, *Polymers*, 2021, **13**, 598.
16. D. Lei, Y. Yang, Z. Liu, B. Yang, W. Gong, S. Chen, S. Wang, L. Sun, B. Song, H. Xuan, X. Mo, B. Sun, S. Li, Q. Yang, S. Huang, S. Chen, Y. Ma, W. Liu, C. He, B. Zhu, E. M. Jeffries, F.-L. Qing, X. Ye, Q. Zhao and Z. You, *Materials Horizons*, 2019, **6**, 1197-1206.
17. A. Salas, M. Zanatta, V. Sans and I. Roppolo, *ChemTexts*, 2023, **9**.
18. B. Toso, M. Gastaldi, G. Renno, C. F. Pirri, C. Barolo, A. Fin and I. Roppolo, *Polymer Chemistry*, 2023, **14**, 1213-1223.
19. E. M. Maines, M. K. Porwal, C. J. Ellison and T. M. Reineke, *Green Chemistry*, 2021, **23**, 6863-6897.
20. M. Shahbazi and H. Jäger, *ACS Applied Bio Materials*, 2021, **4**, 325-369.
21. K. Y. Lee and D. J. Mooney, *Chemical Reviews*, 2001, **101**, 1869-1879.
22. A. J. Engler, S. Sen, H. L. Sweeney and D. E. Discher, *Cell*, 2006, **126**, 677-689.
23. R. Langer and D. A. Tirrell, *Nature*, 2004, **428**, 487-492.
24. W. R. Gombotz and S. F. Wee, *Advanced Drug Delivery Reviews*, 1998, **31**, 267-285.
25. J. A. Rowley, G. Madlambayan and D. J. Mooney, *Biomaterials*, 1999, **20**, 45-53.
26. K. Y. Lee and D. J. Mooney, *Progress in Polymer Science (Oxford)*, 2012, **37**, 106-126.

27. M. E. Furth, A. Atala and M. E. Van Dyke, *Biomaterials*, 2007, **28**, 5068-5073.
28. J. Xu, K. Jung, A. Atme, S. Shanmugam and C. Boyer, *Journal of the American Chemical Society*, 2014, **136**, 5508-5519.
29. X. Hu, Z. Zhang, H. Wu, S. Yang, W. Zhao, L. Che, Y. Wang, J. Cao, K. Li and Z. Qian, *Biomaterials Advances*, 2023, **152**.
30. S. Vanslambrouck, R. Riva, B. Ucar, V. Pr at, M. Gagliardi, D. G. M. Molin, P. Lecomte and C. J r me, *Molecules*, 2021, **26**.
31. H. W. Ooi, C. Mota, A. T. ten Cate, A. Calore, L. Moroni and M. B. Baker, *Biomacromolecules*, 2018, **19**, 3390-3400.
32. R. M. Desai, S. T. Koshy, S. A. Hilderbrand, D. J. Mooney and N. S. Joshi, *Biomaterials*, 2015, **50**, 30-37.
33. J. C. Kloxin, F. T. Scott and N. C. Bowman, *Macromolecules*, 2009, **42**, 2551-2556.
34. C. E. Hoyle and C. N. Bowman, *Angewandte Chemie International Edition*, 2010, **49**, 1540-1573.
35. M. Zanon, L. Montalvillo-Jim nez, P. Bosch, R. Cue-L pez, E. Mart nez-Campos, M. Sangermano and A. Chiappone, *Polymers*, 2022, **14**.
36. H. Choi, M. Kim, J. Jang and S. Hong, *Angewandte Chemie International Edition*, 2020, **59**, 22514-22522.
37. Y. Liu, W. Hou, H. Sun, C. Cui, L. Zhang, Y. Jiang, Y. Wu, Y. Wang, J. Li, B. S. Sumerlin, Q. Liu and W. Tan, *Chemical Science*, 2017, **8**, 6182-6187.
38. A. Oesterreicher, M. Roth, D. Hennen, F. H. Mostegel, M. Edler, S. Kappaun and T. Griesser, *European Polymer Journal*, 2017, **88**, 393-402.
39. A. Bernkop-Schn rch, *Advanced Drug Delivery Reviews*, 2005, **57**, 1569-1582.
40. J. Iqbal, G. Shahnaz, S. D nnhaupt, C. M ller, F. Hintzen and A. Bernkop-Schn rch, *Biomaterials*, 2012, **33**, 1528-1535.
41. Y. Zhang, S. Zhou, F. Deng, X. Chen, X. Wang, Y. Wang, H. Zhang, W. Dai, B. He, Q. Zhang and X. Wang, *European Journal of Pharmaceutics and Biopharmaceutics*, 2018, **133**, 188-199.
42. P. M. Kharkar, M. S. Rehmman, K. M. Skeens, E. Maverakis and A. M. Kloxin, *ACS Biomaterials Science & Engineering*, 2016, **2**, 165-179.
43. C.-C. Lin, A. Raza and H. Shih, *Biomaterials*, 2011, **32**, 9685-9695.
44. R. Holmes, X.-B. Yang, A. Dunne, L. Florea, D. Wood and G. Tronci, *Journal*, 2017, **9**.
45. R. G. Huamani-Palomino, B. M. C rdova, E. R. Pichilingue L, T. Ven ncio and A. C. Valderrama, *Journal*, 2021, **13**.
46. M.  . Dalheim, A. S. T. Ulset, I. B. Jenssen and B. E. Christensen, *Carbohydrate Polymers*, 2017, **157**, 1844-1852.
47. S. Hauptstein, S. Dezorzi, F. Pr ufert, B. Matuszczak and A. Bernkop-Schn rch, *Carbohydrate Polymers*, 2015, **124**, 1-7.
48. Z. Emami, M. Ehsani, M. Zandi and R. Foudazi, *Carbohydr Polym*, 2018, **198**, 509-517.
49. C. M. Q. Le, F. Morlet-Savary and A. Chemtob, *Polymer Chemistry*, 2021, **12**, 6594-6605.
50. D. Schilter, *Nature Reviews Chemistry*, 2017, **1**, 0013.
51. S. W. Griffiths, J. King and C. L. Cooney, *Journal of Biological Chemistry*, 2002, **277**, 25486-25492.
52. J. S. Fritz, S. S. Yamamura and E. C. Bradford, *Analytical Chemistry*, 1959, **31**, 260-263.
53. H. Peng, W. Chen, Y. Cheng, L. Hakuna, R. Strongin and B. Wang, *Sensors*, 2012, **12**, 15907-15946.

54. G. L. Ellman, *Archives of Biochemistry and Biophysics*, 1959, **82**, 70-77.
55. A. Jejurikar, X. T. Seow, G. Lawrie, D. Martin, A. Jayakrishnan and L. Grøndahl, *Journal of Materials Chemistry*, 2012, **22**, 9751-9758.
56. K. H. Bouhadir, K. Y. Lee, E. Alsberg, K. L. Damm, K. W. Anderson and D. J. Mooney, *Biotechnology Progress*, 2001, **17**.
57. C. G. Gomez, M. Rinaudo and M. A. Villar, *Carbohydrate Polymers*, 2007, **67**, 296-304.
58. C. Le-Tien, M. Millette, M. Lacroix and M. A. Mateescu, *Biotechnol Appl Biochem*, 2004, **39**, 189-198.
59. E. W. Baxter and A. B. Reitz, in *Organic Reactions*, DOI: <https://doi.org/10.1002/0471264180.or059.01>, pp. 1-714.
60. P. Di Bernardo, P. L. Zanonato, S. Tamburini, P. Tomasin and P. A. Vigato, *Dalton Transactions*, 2006, DOI: 10.1039/B604211B, 4711-4721.
61. J. Battersby, R. Clark, W. Hancock, E. Puchulu-Campanella, N. Haggarty, D. Poll and D. Harding, *Journal of Controlled Release*, 1996, **42**, 143-156.
62. S. Dünnhaupt, J. Barthelmes, C. C. Thurner, C. Waldner, D. Sakloetsakun and A. Bernkop-Schnürch, *Carbohydr Polym*, 2012, **90**, 765-772.
63. T. F. Palmberger, K. Albrecht, B. Loretz and A. Bernkop-Schnürch, *Eur J Pharm Biopharm*, 2007, **66**, 405-412.
64. E. Guzmán, R. G. Rubio and F. Ortega, *Adv Colloid Interface Sci*, 2020, **282**, 102197.
65. A. Hansson, N. Hashom, F. Falson, P. Rousselle, O. Jordan and G. Borchard, *Carbohydr Polym*, 2012, **90**, 1494-1500.
66. S. Bian, M. He, J. Sui, H. Cai, Y. Sun, J. Liang, Y. Fan and X. Zhang, *Colloids Surf B Biointerfaces*, 2016, **140**, 392-402.
67. J. C. Breger, B. Fisher, R. Samy, S. Pollack, N. S. Wang and I. Isayeva, *J Biomed Mater Res B Appl Biomater*, 2015, **103**, 1120-1132.
68. B. Huber, K. Borchers, G. E. Tovar and P. J. Kluger, *J Biomater Appl*, 2016, **30**, 699-710.
69. M. Zanon, R. Cue-López, E. Martínez-Campos, P. Bosch, D.-L. Versace, H. Hayek, N. Garino, C. F. Pirri, M. Sangermano and A. Chiappone, *Additive Manufacturing*, 2023, **69**, 103553.
70. Z. Feng, M. Hakkarainen, H. Grützmacher, A. Chiappone and M. Sangermano, *Macromolecular Chemistry and Physics*, 2019, **220**, 1900174.
71. C. Noè, C. Tonda-Turo, A. Chiappone, M. Sangermano and M. Hakkarainen, *Polymers*, 2020, **12**, 1359.
72. S. Kim, S. Jung, *Carbohydrates Polymers*, 2020, **250**, 116934.
73. A. M. Handorf, Y. Zhou, M. A. Halanski and W. J. Li, *Organogenesis*, 2015, **11**, 1-15.
74. A. D. Doyle, R. J. Petrie, M. L. Kutys and K. M. Yamada, *Current Opinion in Cell Biology*, 2013, **25**, 642-649.
75. P. Friedl, E. Sahai, S. Weiss and K. M. Yamada, *Nature Reviews Molecular Cell Biology*, 2012, **13**, 743-747.